Charge Carriers Modulate The Bonding Of Semiconductor Nanoparticle Dopants As Revealed By Time-Resolved X-Ray Spectroscopy

Journal:	*ACS Nano*
Manuscript ID	nn-2017-044145.R2
Manuscript Type:	Article
Date Submitted by the Author:	24-Aug-2017

Complete List of Authors:	Hassan, Asra; University of Illinois at Chicago, Chemistry Zhang, Xiaoyi; Argonne National Laboratory, X-ray Science Division Liu, Xiaohan; University of Illinois at Chicago, Chemistry Rowland, Clare; Northwestern University, Chemistry Jawaid, Ali; University of Illinois at Chicago, Chemistry Chattopadhyay, Soma; Elgin Community College, Physical Sciences Gulec, Ahmet; Northwestern University, Material science and Engineering Shamirian, Armen; University of Illinois at Chicago, Chemistry Zuo, Xiaobing; Argonne National Laboratory, X-ray Science Division Klie, Robert; University of Illinois - Chicago, Department of Physics Schaller, Richard; Northwestern University, Department of Chemistry Snee, Preston; University of Illinois, Chicago, Chemistry

Charge Carriers Modulate The Bonding Of Semiconductor Nanoparticle Dopants As Revealed By Time-Resolved X-Ray Spectroscopy

Asra Hassan[†], *Xiaoyi Zhang*[‡], *Xiaohan Liu*[†], *Clare E. Rowland*[§], *Ali M. Jawaid*[†], *Soma Chattopadhyay*[‡], *Ahmet Gulec*[‖], *Armen Shamirian*[†], *Xiaobing Zuo*[‡], *Robert F. Klie*[‖], *Richard D. Schaller*[§,⊥], *Preston T. Snee*[†]*

[†]Department of Chemistry, University of Illinois at Chicago, 845 W. Taylor Street, Chicago, Illinois 60607-7061, USA.

[‡]X-ray Science Division, Argonne National Laboratory, Argonne, IL 60439, USA.

[§]Department of Chemistry, Northwestern University, 2145 Sheridan Road, Evanston, Illinois, 60208-3113, USA.

[‖]Department of Physics, University of Illinois at Chicago, 845 W. Taylor Street, Chicago, Illinois 60607-7061, United States [⊥]Center of Nanoscale Materials, Argonne National Laboratory, Argonne, IL 60439

KEYWORDS semiconductor, nanoparticle, quantum dot, cadmium sulfide, X-ray absorption, doping.

ABSTRACT

Understanding the electronic structure of doped semiconductors is essential to realize advancements in electronics and in the rational design of nanoscale devices. Reported here are the results of time-resolved X-ray absorption studies on copper-doped cadmium sulfide nanoparticles that provide an explicit description of the electronic dynamics of the dopants. The interaction of a dopant ion and an excess charge carrier is unambiguously observed *via* monitoring the oxidation state. The experimental data combined with DFT calculations demonstrate that dopant bonding to the host matrix is modulated by its interaction with charge carriers. Furthermore, the transient photoluminescence and the kinetics of dopant oxidation reveal the presence of two types of surface-bound ions that create mid-gap states.

Generally, intrinsic semiconductors must be modified by the incorporation of dopants into the matrix to add (subtract) electrons to the conduction (valence) bands to create diodes and transistors that are the basis of modern electronics.[1] However, the conduction of charge carriers is impeded by scattering off dopants, which is detrimental to device performance.[2,3] To study semiconductor dopant photophysics, we have examined the transient interaction of an excess charge carrier with a guest ion in a semiconductor matrix using time resolved X-ray absorption spectroscopy (TR-XAS).[4-7] Several synthetic and experimental developments were realized to successfully perform such studies. For example, TR-XAS requires a large quantity of the substrate to flow through a liquid jet to avoid the buildup of oxidized byproducts.[4] To this end, we have developed a method for producing large batches of Cu-doped colloidal CdS semiconductor nanocrystals (NCs, or quantum dots) where each NC contains the exact same number of guest ions. This procedure is based on the cluster seed method, where nanocrystals are nucleated around a small organometallic cluster in a process that can be easily increased in scale.[8-10] Doped NCs are created by the use of a seed that contains the guest ion(s). Furthermore, the method resolves the problems associated with dopant loading level Poissonian inhomogeneity.[11,12]

The results discussed below provide an unambiguous demonstration of hole capture by the dopant due to the fact that photoexcitation of copper-doped cadmium sulfide nanoparticles resulted in a shift of the Cu K-edge X-ray absorption near edge spectroscopy (XANES) absorption to higher energy. This in turn instigated a stronger bonding interaction of copper with sulfur within the semiconductor host as revealed by the excited state extended X-ray absorption fine structure (EXAFS) spectrum. X-ray analyses also revealed two types of surface-bound copper ions that display different dynamics in the excited state. These data were augmented with large-scale Density Functional Theory (DFT) calculations on ground and excited states of quantum dots.[13] Furthermore, the DFT results attest to the generality of the conclusions made with copper-doped CdS dots. Overall, the modulation of dopant bonding by electrons and holes has implications for understanding the dynamics of charge carriers in semiconductor hosts.

RESULTS AND DISCUSSION

Doped Quantum Dots. Doped colloidal semiconductor nanocrystals have been the subject of intense study, as incorporation of guest ions allows for refinement of materials' properties beyond that afforded by quantum confinement effects.[11,12, 14-18] Copper-doped cadmium chalcogenide NCs have been of special interest as holes are hypothesized to localize on copper.[19-22] This paradigm is supported by the observation of NC size-dependent dopant emission that shifts in accordance with the electron energy levels. However, in our previous propose that emission is due to copper-bound electrons recombining with NC holes.[8] Clearly, indirect methods of observation will have some ambiguity in interpretation. For this reason we sought to directly measure the oxidation state of a dopant in a semiconductor host matrix that contains free charge carriers created by photoexcitation. To this end, the cluster seed method was employed due to the method's ability to create a large quantity of homogeneous materials.

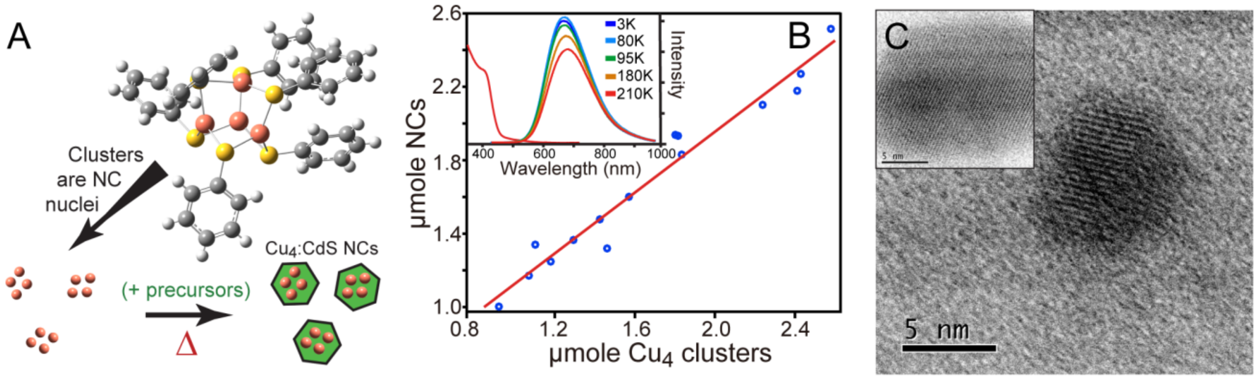

Figure 1. (a) Schematic of the cluster seed method (Color code: orange, copper; yellow, sulfur; grey, carbon; white, hydrogen). (b) The number of clusters used in the synthesis is highly correlated to the quantity of nanocrystals produced. Inset: Absorption (left) and emission (right) spectra of Cu_4:CdS NCs. (c) High resolution TEM micrographs of Cu_4:CdS NCs. Inset scalebar: 5 nm.

The cluster seed protocol was optimized to synthesize cadmium sulfide nanocrystals doped with four copper ions. Among the many characterizations performed, one of the simplest yet powerful demonstrations is the linear relationship that exists between the number of seeds used and the ~ 5 nm quantum dots synthesized as shown in Figure 1. Furthermore, there is no evidence of emission from undoped NCs as the photoluminescence is dominated by sub-bandgap fluorescence. The X-ray absorption onset, lack of magnetism as revealed by SQUID measurements, and phosphorescent emission are consistent with copper dopants in the +1 oxidation state. Several other characterizations were performed, including high resolution electron microscopy, X-ray photoelectron spectroscopy (XPS), X-ray diffraction (XRD), small angle X-ray scattering (SAXS), scanning transmission electron microscopy-electron energy loss spectroscopy (STEM-EELS), and elemental analysis, all of which indicated doped Cu_4:CdS NCs, see Figures 1 & 2 and additional data in the supporting information. Moreover, the nanocrystals are not photooxidized as confirmed by emission and static XANES spectroscopies as shown in Figure S7, which allowed for the use of TR-XAS to study guest-host interactions.[4]

XANES: Oxidation in the excited state. Ultrafast time-resolved X-ray absorption experiments were performed at the beamline 11-ID-D of the Advanced Photon Source at Argonne National Laboratory. The 400 nm laser pulses were stretched to 1.5 ps to negate multiphoton absorption effects as evident from the lack of non-linear power dependence to the data; see the supporting information Figure S9. Optical excitation was followed by X-ray interrogation at specific time delays to measure the Cu-K edge XANES and EXAFS spectra. Shown in Figure 2B are the difference absorption spectra (*i.e.* $Abs_{pump\_on}(\tau) - Abs_{pump\_off}$) at various time delays. These data were used to construct the excited state XANES and EXAFS spectra by adding the appropriately-weighted difference spectrum to the static. The result is shown in Figure 2C, demonstrating that the XANES absorption edge is blue-shifted by ~0.8 eV in the excited state. There is a pre-edge transition observed at 8978 eV, which originates from an electric quadrupole transition from the 1s to vacant 3d orbitals. The 1s to 3d transition feature here unequivocally demonstrate that copper dopants are oxidized to Cu(2+) by the exciton *via* the capture of holes because Cu(1+) and Cu(0) have no vacant 3d orbitals. The main edge transition between 8988 – 8997 eV corresponds to excitation from 1s $\rightarrow$ 4p unoccupied orbitals. The strong absorption at the rising edge peaked around 8982 eV is ascribed to a 1s $\rightarrow$ {4p + shakedown} transition.[23-25] The significant reduced intensity of this transition after excitation suggests increased 3d-4p hybridization. Stronger 3d-4p mixing increases the electron density in the $4p_z$ orbital, thereby reducing the transition intensity.[26,27]

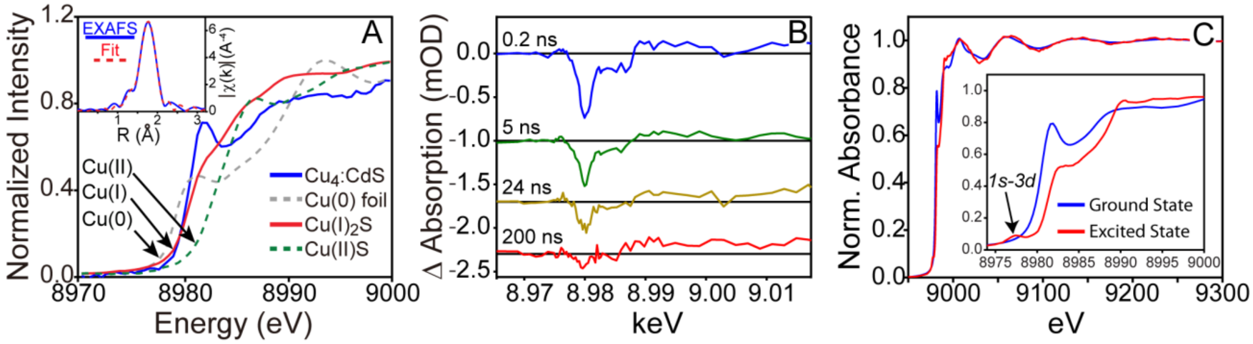

Figure 2. (a) Static Cu K-edge XANES spectra of Cu_4:CdS NCs and various standards demonstrate that copper is in the +1 ground state. Inset: static EXAFS spectrum of Cu4:CdS NCs. (b) TR-XAS difference spectra at the Cu K-edge. (c) The XANES spectra of the ground and excited states of copper in Cu_4:CdS semiconductor nanocrystals. A 1s → 3d pre-edge transition feature is observed at 8978 eV as shown in the inset.

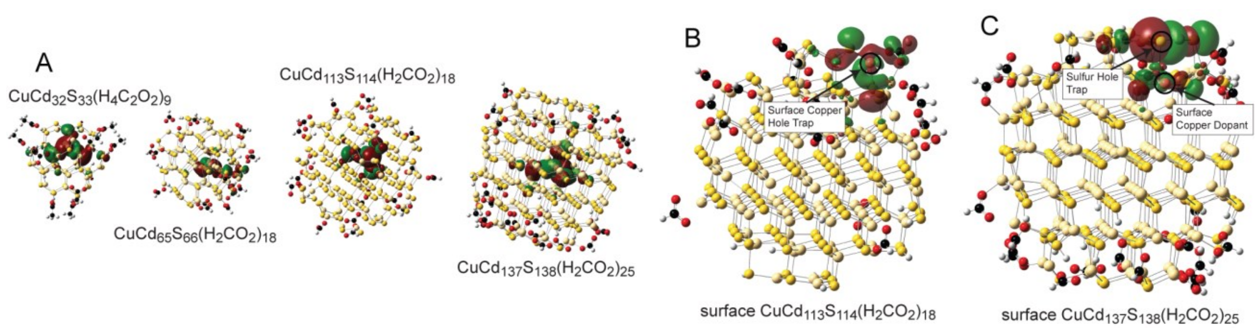

Figure 3. (a) Natural Transition Orbital analysis of the optimized DFT geometries of a size series of interior-doped clusters demonstrates the localization of holes by Cu in the 1st excited state. (b) Optimized DFT geometry of $CuCd_{113}S_{114}(H_2CO_2)_{18}$ where the copper dopant is localized near the surface of the NC. The hole is centered on the dopant in the excited state. (c) Copper near the surface of a larger $CuCd_{137}S_{138}(H_2CO_2)_{25}$ nanocrystal creates a S-centered hole state with some

admixture of Cu character. The "type-II" dopant is not significantly oxidized nor forms a new bond with a nearby S-site in the excited state.

DFT models: Surface and interior-doped NCs. The 1s → 3d pre-edge XANES feature and other absorption shifts are indicative of a modulation of the local structure around the guest ion in the excited state. This prompted us to compare the ground state (*i.e.* static) and the excited state EXAFS spectra, the results from which were augmented with DFT optimized geometries of both the ground and 1^{st} excited (triplet) states of small $CuCd_{32}S_{33}(H_4C_2O_2)_9$ (1.3 nm) to large $CuCd_{137}S_{138}(H_2CO_2)_{25}$ (2.2 nm) clusters, including ligands, as shown in Figure 3A. Natural Bond Orbital (NBO) analyses of the DFT results were employed to assist with describing the bonding and localization of charge in manner similar to a Lewis diagram representation.[28] Both interior and surface doped systems were modeled because the fit to the ground state EXAFS data shown in Table S3 reveal that copper is coordinated with two nearest S-atom neighbors. This strongly suggest that dopants largely reside at the surfaces of CdS NCs,[22, 29] and that copper ions located within the interior must be a minority of the sample population. Such a heterogeneous population likely forms due to the known diffusivity of copper, even through a solid-state material.[30] Regardless, all the systems except the largest surface-doped model discussed below have copper ions that are formally non-bonded to the nearest sulfur sites according to NBO analysis of the ground state. However, oxidation of copper in the 1^{st} excited state results in the formation of bond(s) with one or two of the nearest-neighbor sulfur sites to regain electron density as evident from the ~0.05 Å compression of the Cu-S distances in the excited states' optimized geometries shown in Figure S12 and from NBO analyses.

As stated above, a very different behavior was characterized from DFT calculations of the largest surface-doped $CuCd_{137}S_{138}(H_2CO_2)_{25}$ system. In this "type-II" surface model, copper is flanked by two sulfur sites at 180° as shown in Figures 3C & S13. This coordination environment creates a nearby sulfur-centered hole trap state with only partial Cu character, which negates copper oxidation in the excited state. This also removed the electronic drive for Cu-S bond formation in the excited state. As detailed below, this configuration creates a surface defect-type emission (*i.e*. deep-trap state) yet does not significantly contribute to the TR-XAS signal due to the fact that Cu is not oxidized in the excited state.

EXAFS: Bonding in the excited state. Figure 4A shows the Cu-K edge EXAFS ground and excited state spectra of the doped nanomaterials. The oscillation period in the excited state is shorter, potentially indicating that the Cu-S bond has expanded upon excitation. However, this is contradictory to the fact that copper should form shorter Cu-S bonds in the excited state due to oxidation of the dopant,[31] which is confirmed by the appearance of the1s-3d transition peak, the blue shift of the transition edge in the excited state XANES spectrum, and the DFT results. We propose that this paradox is due to heterogonous Cu-S bond dynamics resulting from the existence of surface and interior copper species as predicted by DFT and corroborated by the kinetic behavior. Two types of Cu-S bond have different structural responses upon photoexcitation, and the interferences created from the two oscillations may lead to an apparent overall shorter oscillation period. We conducted simulations to test this hypothesis. According to DFT calculations, the type-II surface Cu-S bonds do not rearrange in the excited state as shown in Figure S13. This prompted us to simulate a series of EXAFS spectra with scattering contributions from two types of Cu-S bonds that including a shrinking interior Cu-S bond and a static surface bond. Figure S10 shows one example of these simulated ground state and excited state spectra, the results of which show a similar effect (a shortening oscillation period) as observed in the experimental data.

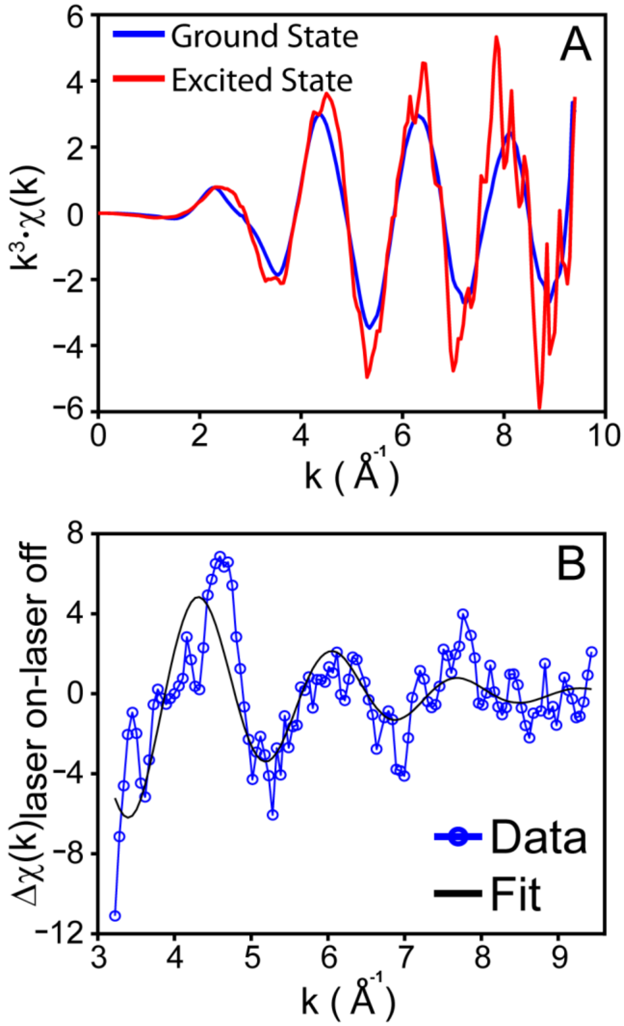

Figure 4. (a) EXAFS k-space spectra of the ground and excited states. (b) The ground to excited state difference EXAFS spectrum and the best fit demonstrate a shortening of the Cu-S bond length.

It is challenging to directly extract excited state structural parameters using conventional X-ray absorption data analysis due to this heterogeneity. Assuming static surface Cu-S bonds, the net change in the EXAFS spectrum is only defined by the absorption difference with the interior Cu-S bond, $A \times [\mu_{excited}^{inter.}(k) - \mu_{ground}^{inter.}(k)]$, where μ is the experimental measured absorption coefficient and A is a constant. This approach allowed us to determine the Cu-S bond lengths. Due to the fact that the pump_on and pump_off spectra were measured simultaneously, it was assumed that they have the same background absorption. Therefore, $[\mu_{excited}^{inter.}(k) - \mu_{ground}^{inter.}(k)] = [\chi_{excited}^{inter.}(k) - \chi_{ground}^{inter.}(k)]$. Figure 4B shows the data and the best fit to the difference spectrum. The average interior Cu-S bond lengths for ground and excited state were determined to be 2.40 ± 0.02 Å and 2.32 ± 0.02 Å, respectively, from the best fit. Note that the 0.08 Å bond compression in the excited state is similar to that predicted by DFT.

Overall, these data demonstrate that copper is oxidized in the excited state which instigates a shortening of the Cu-S bond length for interior-bound guest ions. This is consistent with the DFT data that dictate that interaction of the dopant with the excess charge carrier results in a modulation of the dopant bonding to the semiconductor host matrix. Such an interaction a phenomenon that is akin to small polaron dynamics as the modulation of dopant ion bonding induced by interaction with a charge carrier likely results in lower charge carrier mobility.[32-34] To examine the generality of this phenomenon, additional guest / host systems were theoretically investigated, including Cu doped CdSe, ZnSe, InAs, InP. It was found that interaction of charge carriers modulated the bonding of the dopant in the excited state in every model system. The impact of the effect was found to be dependent on the valence potential of the host, as copper is less oxidized and subsequently has weaker bonding to a matrix with a higher energy valence state. The effect of electron capture by a guest ion was also studied using an indium-doped $InCd_{65}S_{66}(H_2CO_2)_{18}$ cluster model. Indium is bonded to four nearest neighbor S-sites in the ground state. However, in the 1st excited state the dopant is reduced which ruptures a bond with one of the nearest neighbor sulfur atoms; see the supporting information for further details. The effect of carrier-modulated dopant bonding can also be mollified or enhanced by tailoring the material system. To demonstrate, the four nearest neighbors of an interior doped $CuCd_{65}S_{66}(H_2CO_2)_{18}$ model were replaced with either oxygen or selenium. It was found that the extent of rebonding in the excited state was significantly reduced with selenium nearest neighbors, while the opposite was true with oxygen as shown in Figure S15. This information may allow for the design of materials to tune the dopant – charge carrier interaction and potentially reduce scattering. Furthermore, the cluster seeded doping method may allow for the experimental realization of such advanced materials as we demonstrated in our previous publication that the cluster seed remains partially intact during QD synthesis.[8]

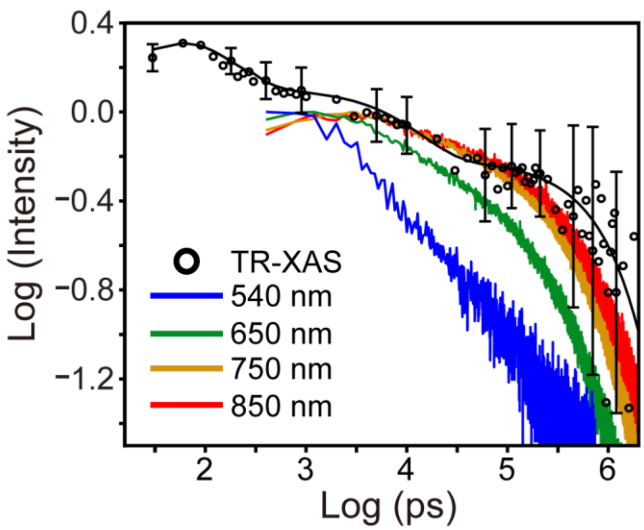

Figure 5. Copper oxidation kinetics compared to time-resolved emission dynamics at different probe wavelengths.

Oxidation and PL dynamics. The kinetics of dopant oxidation shown in Figure 5 reveal significant complexity as they are only partially consistent with the time-resolved photoluminescence data. There is an initial sub-ns relaxation that is not observed in the photoluminescence data at any wavelength. This dynamic must originate from the recombination of electrons with oxidized surface-bound copper for several reasons, including the fact that surface-doping pre-formed QDs with copper results in significant fluorescence quenching. Furthermore, the EXAFS fitting was consistent with a population of surface-dopant species. This non-radiative recombination is followed by short ~10 ns and longer ~1 μs timescale components that have analogs in the photoluminescence data. Most likely these are the radiative dynamics of interior-bound copper recombining with excitonic and surface-trapped electrons. What is very curious is that there is a ~100 ns dynamic in the photoluminescence that is not observed in the TR-XAS data. As this timescale is very similar to that observed from electron-hole recombination at charge-trapping surface states,[35,36] and the fact that DFT modeling reveal that dopants may not be significantly redox active if they generate hole-trapping surface states,[35] this dynamic is attributed to emission from type-II surface doped copper species. Overall, these data demonstrate that one may not assume that time-resolved dopant-modulated emission tracks the photochemical dynamics of the same species. Rather, the sub-bandgap emission from doped semiconductors may result from a complex convolution of interior and surface-bound species that may, or may not, have redox active excited state behavior.

CONCLUSION

Time-resolved X-ray absorption spectroscopy coupled with large-scale DFT calculations offer unambiguous insight into the photophysical properties of semiconductor dopants in nanostructures. To conduct this study, large batches of exactly doped Cu_4:CdS NCs samples were synthesized via the cluster seeding method. Although highly effective, the population of copper ions are found to be divided between interior doped and two types of surface-bound species. A microscopic picture of the electronic structure of these guest ions in the presence of charge carriers was obtained, the dynamics of which demonstrate that dopant bonding is modulated by free charge carriers. Note that there were some differences in the dynamics of interior dopants vs. the surface-bound ions. We believe that a variety of doped semiconductor materials display these dynamics, which likely impacts charge transport characteristics of QD "artificial solids" and even bulk materials due to chemical trapping of charge carriers at dopant sites. These results demonstrate the necessity of using powerful techniques such as TR-XAS to generate a comprehensive understanding of the electronic structure and dynamics of advanced materials.

EXPERIMENTAL

Materials. 1-Octadecene (90%), oleylamine (90%), benzenethiol (97%), anhydrous methanol (99.8%), trimethylamine (97%), tetramethylammonium chloride (97%), cadmium acetate (99.999%), and thiourea (99%) were purchased from Sigma-Aldrich. Anhydrous dimethylformamide (DMF, 99.8%) and copper (II) nitrate trihydrate (99%) were purchased from Acros. 1-Butanol (95%) was purchased from Strem. Oleylamine was purified by recrystallization at -30 ºC from acetonitrile and was stored at 4 ºC. All other reagents were used without further purification.

Methods. CdS:Cu_4 synthesis using $[N(Me_4)]_2[Cu_4(SPh)_6]$ as seeds. Into a 50 mL three-neck flask, 7 mL of 1-octadecene, 2 mL of purified oleylamine, and 0.23 g (1 mmol) of cadmium acetate were added and heated to 110 °C under vacuum for 1 hr. The solution turned clear and the vessel was backfilled with N_2 and cooled to room temperature. Next, 0.8-2.8 mg of $[N(Me_4)]_2[Cu_4(SPh)_6]$ dissolved into a minimal amount of DMF (~0.1 mL) was added at room temperature into the degassed solvent, followed by 0.038 g (0.5 mmol) thiourea in a minimal amount of DMF (~0.5 mL) and 2 mL of 1-butanol. The solution was slowly heated to 50 °C and monitored *via* absorption for 1 hr. Finally, the solution was heated gradually to 100 °C at a rate of 5 °C / min, and was maintained at this temperature for ~16 hrs.

TR-XAS. Time-resolved Cu K-edge XANES measurements (TR-XAS) were performed in total fluorescence mode at beamline 11-ID-D of the Advanced Photon Source, Argonne National

Laboratory. The laser pump pulse was the second harmonic output of a Ti:Sapphire regenerative amplified laser with 10 kHz repetition rate, giving 400 nm laser pulses with 500 fs FWHM. The laser pulse was further stretched to 1.5 ps using a prism pair. The experiment was carried out under the hybrid-timing mode where an intense X-ray pulse was used as the probe pulse. This intense pulse (117 ps, 271.5 kHz) contains 16% of the total average photon flux and was separated in time from other weak X-ray pulses. A ~0.33 mM suspension of quantum dots was pumped through a stainless-steel tube to create a 600 μm diameter free jet. Two avalanche photodiodes (APDs) positioned at 90˚ on both sides of the incident X-ray beam collected the X-ray fluorescence signals. A soller slit and an additional Ni filter of 6 absorption length combination was inserted between the sample fluid jet and the APD detectors to block the scattering background. The outputs of the APDs were sent to a fast analyzer card (Agilent) triggered by a 10 kHz signal that is synchronized with the laser pulse. The card digitized the X-ray fluorescence signals as a function of time at 1 ns per point after each trigger and averaged repeated measurements using 4 s integration time. The fluorescence from the synchronized X-ray pulse at chosen delays after the laser excitation was used for creating the excited state spectrum. The ground state spectrum was obtained by averaging X-ray pulses in the previous 20 synchrotron ring cycles.

The synchronization between the laser and X-ray was achieved using a fast diode (“sample diode”) with a 40 ps rise time positioned where X-ray and laser spatially overlap. The output of the sample diode was connected to an oscilloscope (Agilent, Infiniium, 8 GHz 20/40 GSa). The output trace of the sample diode was recorded with only the laser signal or X-ray input separately, then the delay between the laser and X-ray was adjusted until the signal traces from laser and X-ray overlaps on the screen of the oscilloscope. The delay was adjusted using a programmable delay line (PDL-100A-20NS, Colby Instruments) that modulated the phase shift of the mode-lock driver for the seed laser relative to that of the RF signal of the storage ring with a precision of 500 fs. The precision of delay measurement is less than 10 ps.

The excited state X-ray spectra were created by adding the difference spectrum, increased by a specific weight (ω), to the ground state spectrum. This composition is conceptually described in Figure S8, where the effect of weighting factors of 20×, 30×, and 40× are represented. Note that a factor of ω=20× was used in the data presented in Figure 2C & 4. The excited state spectra were constructed from data obtained at a delay of 90 ps. The kinetic trace shown in Figure 5 was obtained by monitoring the magnitude of the X-ray absorption bleach at 8982 eV over various time delays.

EXAFS data analysis. The excited state is EXAFS spectrum was constructed by adding 20× difference spectrum (*i.e.*, pump_on – pump_off) to the ground state spectrum to better illustrate the change in the excited state.

Experimental data reduction. The Athena program was used to process ground state X-ray absorption data to extract the normalized oscillation amplitude in the ground state $\chi_{ground}^{exp}(k)$. Here, k is the photoelectron wave number as defined by $k = \sqrt{2m(E - E_0)}$, where E_0 is the absorption edge energy, m is the eletron mass, and $\hbar$ is the reduced Plank constant. Because the ground state and "pump_on" spectra were measured simutaneously, it is reaonable to assume that they have the same background aborption. Therefore, the same background as the ground state spectrum was used to extract $\chi_{excited}^{exp}(k)$ from the "pump_on" spectrum.

EXAFS data fitting. The theoretical oscillation amplitude of the X-ray absorption spectrum, $\chi^{theory}(k)$, is determined using the EXAFS equation: $\chi^{theory}(k) = \sum_j \frac{S_0^2 N_j f_j(k)}{kR_j^2} e^{-2k^2\sigma_j^2} e^{-2r_j/\lambda(k)} \sin[2kR_j + \delta_j(k, r_j)]$ where j indicates a shell with identical backscatters, N_j is the coordination number of the j^{th} shell, f_j is the backscattering amplitude, R_j is the average distance, σ_j is the mean square variation, δ_j is the scattering phase shift, λ is the effective mean free path, and S_0^2 is the amplitude reduction factor. In this manuscript, only the first Cu-S coordinate shell were used to calculate $\chi(k)$. Concerning the fit to the difference spectrum, in-house Perl scripts incorporating FEFF 9.05 were used to calculate f_j, N_j, δ_j and λ, while the structure parameters S_0^2, R_j, σ_j^2, and E_0 were refined by fitting the experimental data. E_0 were refined by fitting the experimental data. The difference spectrum fitting only included the path of the first Cu-S coordination shell. The ground and excited states shared a common S_0^2. The σ^2 was obtained by fixing the temperature at 300 K (*i.e.* room temperature) and fitting the Debye temperature.

DFT. Density Functional Theory (DFT) modeling of small to large doped semiconductor clusters was performed using the PBE1/PBE hybrid functional,[37,38] with the SBJKC basis set and effective core potentials (ECPs).[39] Very large clusters employed the LANL2DZ basis set and ECPs[40-42] in NBO analyses. Cluster sizes varied from $CuCd_{32}S_{33}(H_4C_2O_2)_9$ to $CuCd_{137}S_{138}(H_2CO_2)_{25}$. The paradigm of Stener and co-workers was used to generate initial geometries, especially is it pertains to the surface ligand structure.[43] Other copper-doped semiconductors matrices, $H_{38}CuZn_{116}Se_{117}$, $H_{38}CuIn_{116}P_{117}$, and $H_{38}CuIn_{116}As_{117}$, were modeled with hydrogen termination in lieu of formic or acetic acid ligands used for other clusters. Although the synthesized CdS:Cu_4 QDs were capped with oleylamine, the use of amine ligands for DFT electronic structure calculations is not preferred.[43] All models had a net single negative charge to assure a singlet spin in the ground state, except for the indium complex $InCd_{65}S_{66}(H_2CO_2)_{18}$ that was modeled with a net single positive charge to account for the loss of electron density upon replacement of an In(+3) site with Cd(+2). Undoped clusters were also studied, all of which were modeled as neutral and singlet. Gaussian ’09 was used for the structure refinement and DFT, including TD-DFT, calculations,[44] as well as natural transition orbital (NTO) analyses of the excited states.[45] The Natural Bonding Orbital (NBO) 6.0 package was used to analyze electron and hole localization in the excited states as well as bonding patterns.[28] Visualization was performed using GaussView.[46] These calculations were run over several months on UIC’s Extreme Computing Cluster. All geometries were examined and re-optimized in some instances to assure that surface states are passivated by ligands.

ASSOCIATED CONTENT

Supporting Information. Additional characterization data on QDs such as optical, elemental analysis, high resolution electron microscopy, XPS, XRD, SAXS, and STEM-EELS as well additional X-ray absorption measurements and DFT calculations. The Supporting Information is available free of charge on the ACS Publications website.

Corresponding Author

* sneep@uic.edu.

Author Contributions

The manuscript was written through contributions of all authors.

Funding Sources

The University of Illinois at Chicago and the U.S. Department of Energy.

ACKNOWLEDGMENT

We would like to thank Jordi Cabana for XRD measurements, Tad Daniel for XPS measurements, and Adita Das for assistance with X-ray data collection. Joseph Zadrozny and Danna Freedman for assistance with SQUID magnetometry measurements as well as data analysis. Mauro Stener and Mauro Del Ben for providing initial nanoparticle geometries for DFT modeling. Eric Glendening and Frank Weinhold for modifying the NBO 6.0 software package for analysis of large cluster structures. Startup funding to PTS from the University of Illinois at Chicago supported this work. This research used resources of the Advanced Photon Source, a U.S. Department of Energy (DOE) Office of Science User Facility operated for the DOE Office of Science by Argonne National Laboratory under Contract No. DE-AC02-06CH11357.

REFERENCES

1. Bardeen, J.; Brattain, W. H. The Transistor, A Semi-Conductor Triode. *Phys. Rev.* **1948**, *74*, 230-231.

2. Conwell, E.; Weisskopf, V. F. Theory of Impurity Scattering in Semiconductors. *Phys. Rev.* **1950**, *77*, 388-390.

3. Chattopadhyay, D.; Queisser, H. J. Electron Scattering by Ionized Impurities in Semiconductors. *Rev. Mod. Phys.* **1981**, *53*, 745-768.

4. Chen, L. X.; Zhang, X. Photochemical Processes Revealed by X-ray Transient Absorption Spectroscopy. *J. Phys. Chem. Lett.* **2013**, *4*, 4000-4013.

5. Chen, L. X.; Jäger, W. J. H.; Jennings, G.; Gosztola, D. J.; Munkholm, A.; Hessler, J. P. Capturing a Photoexcited Molecular Structure Through Time-Domain X-ray Absorption Fine Structure. *Science* **2001**, *292*, 262-264.

6. Saes, M.; Bressler, C.; Abela, R.; Grolimund, D.; Johnson, S. L.; Heimann, P. A.; Chergui, M. Observing Photochemical Transients by Ultrafast X-ray Absorption Spectroscopy. *Phys. Rev. Lett.* **2003**, *90*, 047403.

7. Bressler, C.; Chergui, M. Molecular Structural Dynamics Probed by Ultrafast X-Ray Absorption Spectroscopy. *Annu. Rev. Phys. Chem.* **2010**, *61*, 263-282.

8. Jawaid, A. M.; Chattopadhyay, S.; Wink, D. J.; Page, L. E.; Snee, P. T. Cluster-Seeded Synthesis of Doped CdSe:Cu_4 Quantum Dots. *ACS Nano* **2013**, *7*, 3190-3197.

9. Pickett, N. (Nanoco Technologies Limited, GB) Controlled Preparation of Nanoparticle Materials. U.S. Patent 7,867,556, October 27, 2006.

10. Santiago-González, B.; Monguzzi, A.; Pinchetti, V.; Casu, A.; Prato, M.; Lorenzi, R.; Campione, M.; Chiodini, N.; Santambrogio, C.; Meinardi, F.; Manna, L.; Brovelli, S. "Quantized" Doping of Individual Colloidal Nanocrystals Using Size-Focused Metal Quantum Clusters. *ACS Nano* **2017**, *11*, 6233–6242.

11. Mocatta, D.; Cohen, G.; Schattner, J.; Millo, O.; Rabani, E.; Banin, U. Heavily Doped Semiconductor Nanocrystal Quantum Dots. *Science* **2011**, *332*, 77-81.

12. Chikan, V. Challenges and Prospects of Electronic Doping of Colloidal Quantum Dots: Case Study of CdSe. *J. Phys. Chem. Lett.* **2011**, *2*, 2783-2789.

13. Nelson, H. D.; Li, X. S.; Gamelin, D. R. Computational Studies of the Electronic Structures of Copper-Doped CdSe Nanocrystals: Oxidation States, Jahn-Teller Distortions, Vibronic Bandshapes, and Singlet-Triplet Splittings. *J. Phys. Chem. C* **2016**, *120*, 5714-5723.

14. Erwin, S. C.; Zu, L.; Haftel, M. I.; Efros, A. L.; Kennedy, T. A.; Norris, D. J. Doping Semiconductor Nanocrystals. *Nature* **2005**, *436*, 91-94.

15. Meulenberg, R. W.; van Buuren, T.; Hanif, K. M.; Willey, T. M.; Strouse, G. F.; Terminello, L. J. Structure and Composition of Cu-Doped CdSe Nanocrystals Using Soft X-ray Absorption Spectroscopy. *Nano Lett.* **2004**, *4*, 2277-2285.

16. Beaulac, R.; Schneider, L.; Archer, P. I.; Bacher, G.; Gamelin, D. R. Light-Induced Spontaneous Magnetization in Doped Colloidal Quantum Dots. *Science* **2009**, *325*, 973-976.

17. Pradhan, N.; Goorskey, D.; Thessing, J.; Peng, X. G. An Alternative of CdSe Nanocrystal Emitters: Pure and Tunable Impurity Emissions in ZnSe Nanocrystals. *J. Am. Chem. Soc.* **2005**, *127*, 17586-17587.

18. Viswanatha, R.; Brovelli, S.; Pandey, A.; Crooker, S. A.; Klimov, V. I. Copper-Doped Inverted Core/Shell Nanocrystals with "Permanent" Optically Active Holes. *Nano Lett.* **2011**, *11*, 4753-4758.

19. Knowles, K. E.; Hartstein, K. H.; Kilburn, T. B.; Marchioro, A.; Nelson, H. D.; Whitham, P. J.; Gamelin, D. R. Luminescent Colloidal Semiconductor Nanocrystals Containing Copper: Synthesis, Photophysics, and Applications. *Chem. Rev.* **2016**, *116*, 10820-10851.

20. Grandhi, G. K.; Tomar, R.; Viswanatha, R. Study of Surface and Bulk Electronic Structure of II–VI Semiconductor Nanocrystals Using Cu as a Nanosensor. *ACS Nano* **2012**, *6*, 9751-9763.

21. Srivastava, B. B.; Jana, S.; Pradhan, N. Doping Cu in Semiconductor Nanocrystals: Some Old and Some New Physical Insights. *J. Am. Chem. Soc.* **2011**, *133*, 1007-1015.

22. Gul, S.; Cooper, J. K.; Glans, P. A.; Guo, J. H.; Yachandra, V. K.; Yano, J.; Zhang, J. Z. Effect of Al^{3+} Co-doping on the Dopant Local Structure, Optical Properties, and Exciton Dynamics in Cu^{+}-Doped ZnSe Nanocrystals. *ACS Nano* **2013**, *7*, 8680-8692.

23. Kau, L. S.; Spira-Solomon, D. J.; Penner-Hahn, J. E.; Hodgson, K. O.; Solomon, E. I. X-ray Absorption Edge Determination of the Oxidation State and Coordination Number of Copper. Application to the Type 3 Site in Rhus Vernicifera Laccase and Its Reaction with Oxygen. *J. Am. Chem. Soc.* **1987**, *109*, 6433-6442.

24. Bocharov, S.; Kirchner, T.; Dräger, G.; Šipr, O.; Šimůnek, A. Dipole and Quadrupole Contributions to Polarized Cu K X-ray Absorption Near-edge Structure Spectra of CuO. *Phys. Rev. B* **2001**, *63*, 045104.

25. Yokoyama, T.; Kosugi, N.; Kuroda, H. Polarized XANES Spectra of $CuCl_2.2H_2O$ - Further Evidence For Shake-Down Phenomena. *Chem. Phys.* **1986**, *103*, 101-109.

26. Blackburn, N. J.; Strange, R. W.; Farooq, A.; Haka, M. S.; Karlin, K. D. X-ray Absorption Studies of Three-Coordinate Dicopper(I) Complexes and their Dioxygen Adducts. *J. Am. Chem. Soc.* **1988**, *110*, 4263-4272.

27. Mara, M. W.; Jackson, N. E.; Huang, J.; Stickrath, A. B.; Zhang, X.; Gothard, N. A.; Ratner, M. A.; Chen, L. X. Effects of Electronic and Nuclear Interactions on the Excited-State Properties and Structural Dynamics of Copper(I) Diimine Complexes. *J. Phys. Chem. B* **2013**, *117*, 1921-1931.

28. Choi, D.; Pyo, J. Y.; Jang, D. J. Impurity Location-Dependent Relaxation Dynamics of Cu:CdS Quantum Dots. *Nanoscale Res. Lett.* **2017**, 12: 49.

29. Holmberg, V. C.; Collier, K. A.; Korgel, B. A. Real-Time Observation of Impurity Diffusion in Silicon Nanowires. *Nano Lett.* **2011**, *11*, 3803-3808.

30. Glendening, E. D.; Badenhoop, J. K.; Reed, A. E.; Carpenter, J. E.; Bohmann, J. A.; Morales, C. M.; Landis, C. R.; Weinhold, F. *NBO 6.0*, Theoretical Chemistry Institute: University of Wisconsin, Madison, 2013.

31. Johnson, B. J.; Antholine, W. E.; Lindeman, S. V.; Graham, M. J.; Mankad, N. P. A One-Hole Cu_4S Cluster with N_2O Reductase Activity: A Structural and Functional Model for Cu-Z. *J. Am. Chem. Soc.* **2016**, *138*, 13107-13110.

32. Mott, N. F. Metal-Insulator Transition. *Rev. Mod. Phys.* **1968**, *40*, 677-683.

33. Kobashi, M.; Takeuchi, H. Inhomogeneity of Spin-Coated and Cast Non-Regioregular Poly(3-hexylthiophene) Films. Structures and Electrical and Photophysical Properties. *Macromolecules* **1998**, *31*, 7273-7278.

34. Sirringhaus, H.; Brown, P. J.; Friend, R. H.; Nielsen, M. M.; Bechgaard, K.; Langeveld-Voss, B. M. W.; Spiering, A. J. H.; Janssen, R. A. J.; Meijer, E. W.; Herwig, P.; de Leeuw, D. M. Two-Dimensional Charge Transport in Self-Organized, High-Mobility Conjugated Polymers. *Nature* **1999**, *401*, 685-688.

35. Veamatahau, A.; Jiang, B.; Seifert, T.; Makuta, S.; Latham, K.; Kanehara, M.; Teranishi, T.; Tachibana, Y. Origin of Surface Trap States in CdS Quantum Dots: Relationship Between Size Dependent Photoluminescence and Sulfur Vacancy Trap States. *PCCP* **2015**, *17*, 2850-2858.

36. Hasselbarth, A.; Eychmuller, A.; Weller, H. Detection of Shallow Electron Traps in Quantum Sized CdS by Fluorescence Quenching Experiments. *Chem. Phys. Lett.* **1993**, *203*, 271-276.

37. Adamo, C.; Barone, V. Toward Reliable Density Functional Methods Without Adjustable Parameters: The PBE0 Model. *J. Chem. Phys.* **1999**, *110*, 6158-6170.

38. Perdew, J. P.; Burke, K.; Ernzerhof, M. Generalized Gradient Approximation Made Simple. *Phys. Rev. Lett.* **1996**, *77*, 3865-3868.

39. Stevens, W. J.; Krauss, M.; Basch, H.; Jasien, P. G. Relativistic Compact Effective Potentials and Efficient, Shared-exponent Basis Sets for the Third-, Fourth-, and Fifth-row Atoms. *Can. J. Chem.* **1992**, *70*, 612-630.

40. Hay, P. J.; Wadt, W. R. *Ab Initio* Effective Core Potentials for Molecular Calculations - Potentials for the Transition-metal Atoms Sc To Hg. *J. Chem. Phys.* **1985**, *82*, 270-283.

41. Hay, P. J.; Wadt, W. R. *Ab Initio* Effective Core Potentials for Molecular Calculations - Potentials for K to Au Including the Outermost Core Orbitals. *J. Chem. Phys.* **1985**, *82*, 299-310.

42. Wadt, W. R.; Hay, P. J. *Ab Initio* Effective Core Potentials for Molecular Calculations - Potentials for Main Group Elements Na to Bi. *J. Chem. Phys.* **1985**, *82*, 284-298.

43. Del Ben, M.; Havenith, R. W. A.; Broer, R.; Stener, M. Density Functional Study on the Morphology and Photoabsorption of CdSe Nanoclusters. *J. Phys. Chem. C* **2011**, *115*, 16782-16796.

44. Frisch, M. J.; Trucks, G. W.; Schlegel, H. B.; Scuseria, G. E.; Robb, M. A.; Cheeseman, J. R.; Scalmani, G.; Barone, V.; Mennucci, B.; Petersson, G. A.; Nakatsuji, H.; Caricato, M.; Li, X.; Hratchian, H. P.; Izmaylov, A. F.; Bloino, J.; Zheng, G.; Sonnenberg, J. L.; Hada, M.; Ehara, M. et al. Gaussian 09, Revision B.01; Gaussian, Inc.: Wallingford, CT, 2009.

45. Martin, R. L. Natural Transition Orbitals. *J. Chem. Phys.* **2003**, *118*, 4775-4777.

46. Dennington, Roy; Keith, Todd; Millam, John. *GaussView*, Version 5; Semichem Inc.: Shawnee Mission, KS, 2009.

For Table of Contents Only